JCI insight

Direct activation of PP2A for the treatment of tyrosine kinase inhibitor–resistant lung adenocarcinoma

Rita Tohmé, … , Jaya Sangodkar, Goutham Narla
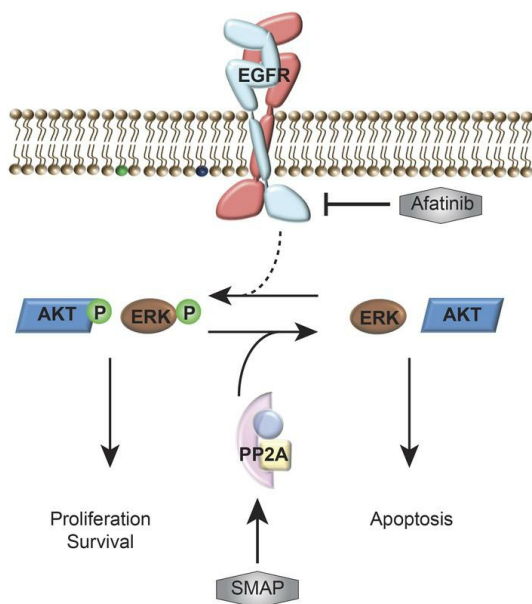
Research Article   Oncology   Therapeutics

Graphical abstract

Find the latest version:

https://jci.me/125693/pdf

Direct activation of PP2A for the treatment of tyrosine kinase inhibitor–resistant lung adenocarcinoma

Rita Tohmé,[1,2] Sudeh Izadmehr,[3] Sai Gandhe,[2] Giancarlo Tabaro,[2] Sanjay Vallabhaneni,[2] Ava Thomas,[2] Neal Vasireddi,[2] Neil S. Dhawan,[4] Avi Ma'ayan,[5] Neelesh Sharma,[6] Matthew D. Galsky,[7] Michael Ohlmeyer,[8] Jaya Sangodkar,[9] and Goutham Narla[9]

[1]Department of Molecular Medicine, Cleveland Clinic, Cleveland, Ohio, USA. [2]Case Comprehensive Cancer Center, Case Western Reserve University, Cleveland, Ohio, USA. [3]Division of Hematology and Medical Oncology, Tisch Cancer Institute, [4]Department of Genetics and Genomic Sciences and [5]Department of Pharmacological Sciences, Icahn School of Medicine at Mount Sinai, New York, USA. [6]University Hospitals Seidman Cancer Center, Case Western Reserve University, Cleveland, Ohio, USA. [7]Department of Medicine and [8]Department of Structural and Chemical Biology, Icahn School of Medicine at Mount Sinai, New York, USA. [9]Division of Genetic Medicine, Department of Medicine, University of Michigan, Ann Arbor, Michigan, USA.

Although tyrosine kinase inhibitors (TKIs) have demonstrated significant efficacy in advanced lung adenocarcinoma (LUAD) patients with pathogenic alterations in EGFR, most patients develop acquired resistance to these agents via mechanisms enabling the sustained activation of the PI3K and MAPK oncogenic pathways downstream of EGFR. The tumor suppressor protein phosphatase 2A (PP2A) acts as a negative regulator of these pathways. We hypothesize that activation of PP2A simultaneously inhibits the PI3K and MAPK pathways and represents a promising therapeutic strategy for the treatment of TKI-resistant LUAD. After establishing the efficacy of small molecule activators of PP2A (SMAPs) in a transgenic EGFR[L858R] model and TKI-sensitive cell lines, we evaluated their therapeutic potential in vitro and in vivo in TKI-resistant models. PP2A activation resulted in apoptosis, significant tumor growth inhibition, and downregulation of PI3K and MAPK pathways. Combination of SMAPs and TKI afatinib resulted in an enhanced effect on the downregulation of the PI3K pathway via degradation of the PP2A endogenous inhibitor CIP2A. An improved effect on tumor growth inhibition was observed in a TKI-resistant xenograft mouse model treated with a combination of both agents. These collective data support the development of PP2A activators for the treatment of TKI-resistant LUAD.

Introduction

As projected by the North American Association of Central Cancer Registries, cancers of the lung continue to be the most common reason for cancer fatalities among both sexes, accounting for more than one-quarter of all cancer deaths (1). Over 40% of lung cancers are lung adenocarcinomas (LUADs), which are most commonly found in outer parts of the lungs (2). Despite advances in diagnosis and therapies, LUAD is characterized by poor prognosis and modest response to therapy, with the average 5-year survival rate for patients with LUAD being 15% (3, 4). A variety of targetable molecular drivers have recently been identified to drive lung cancer progression, with the best example being activating alterations in the tyrosine kinase EGFR in LUAD. Patients with EGFR alterations were found to have increased sensitivity to targeted tyrosine kinase inhibitors (TKIs), such as erlotinib and gefitinib (5, 6). Despite their clinical successes, most patients develop acquired resistance to TKIs within 9–12 months via mechanisms enabling the sustained activation of the MAPK and PI3K oncogenic pathways downstream of EGFR (7–9). The tumor suppressor protein phosphatase 2A (PP2A) acts as a negative regulator of these pathways (10, 11). PP2A is a serine/threonine phosphatase that is implicated in many cellular functions that control growth, metabolism, cell cycle, and apoptosis (12). It is composed of a scaffolding A subunit and the catalytic C subunit that together form the core enzyme. Both the A and C subunits have 2 possible isoforms, α and β, with the α isoforms accounting for the majority of each subunit in most cells. The core enzyme associates with one of many regulatory B subunits responsible for substrate specificity to form the heterotrimeric holoenzyme complex (13–15).

Our lab has successfully developed a published series of first-in-class small molecule activators of PP2A (SMAPs), which directly bind to PP2A and induce apoptosis and tumor growth inhibition in both transgenic and xenograft KRAS-driven mice models (16–18). SMAPs have been generated by repurposing and reengineering FDA-approved tricyclic neuroleptics through replacing the basic amine with a neutral polar functional group (19). In silico docking calculations, hydroxyl radical footprinting studies, and photo-affinity labeling have shown that SMAPs directly bind the scaffolding A subunit of PP2A (17). We believe SMAP binding causes allosteric conformational changes that lead to PP2A activation and the subsequent dephosphorylation of its downstream targets. We hypothesize that activation of PP2A simultaneously inhibits the MAPK and AKT pathways and is a promising therapeutic strategy for TKI-resistant LUAD.

Results

We sought to determine whether activation of PP2A using SMAPs in EGFR-driven TKI-sensitive and TKI-resistant models is a viable therapeutic strategy for the treatment of LUAD. Our initial experiments were performed using one of the first engineered SMAPs in our laboratory, SMAP DT-382 (Supplemental Figure 1A; supplemental material available online with this article; https://doi.org/10.1172/jci.insight.125693DS1). We have subsequently developed a more bioavailable PP2A activator, SMAP DT-061, with higher in vivo potency that we used for ensuing experiments (Supplemental Figure 1B). Both SMAP DT-382 and SMAP DT-061 were shown to have comparable biological effects, target specificity, and a favorable toxicity profile in our previously published work (17).

Administration of SMAP in a TKI-sensitive transgenic mouse model is well tolerated and inhibits lung tumor development. We investigated the effect of PP2A activation on tumorigenesis in TKI-sensitive models to test the ability of these SMAPs to coordinately downregulate MAPK and PI3K signaling in vivo. The therapeutic potential of PP2A reactivation in vivo was first evaluated in a transgenic EGFR/CCSP mouse model. This model contains a human EGFR transgene, TRE-EGFR[L858R], and an activating, transgene-directing expression of mutant EGFR to the Clara cells (6, 20). In this model, treatment with doxycycline activates the transgene and leads the transcription of the L858R-mutant EGFR in the lung. Eight weeks after induction with doxycycline, mice with confirmed tumors observed by small rodent MRI were administered either vehicle control ($n = 3$) or SMAP DT-382 ($n = 3$) via intraperitoneal injection every 48 hours for a total of 5 doses (Figure 1A). SMAP treatment was well tolerated and had no notable toxicities, such as mucous diarrhea or abdominal stiffness. Lung tumor development was monitored by MRI. Mice treated with vehicle control showed diffuse lung cancer and interspersed multifocal adenocarcinomas (Figure 1B). Tumor growth was markedly inhibited in mice treated with SMAP. Mice were sacrificed 2 hours after the last treatment, and H&E-stained sections of lung samples were derived from the lung tissue. The reticulonodular pattern observed with MRI was recapitulated by H&E staining, because fewer nodules were present after treatment in animals from the SMAP arm (Figure 1C). Quantification of MRI (Figure 1D) and H&E (Figure 1E) results showed a significant decrease in total nodules ($P < 0.05$) and tumor volume ($P < 0.05$). Immunohistochemical staining was used to detect the expression markers of apoptosis (TUNEL), proliferation (PCNA), and pERK and pAKT. IHC showed increased TUNEL ($P < 0.001$) and decreased PCNA ($P < 0.001$) staining in SMAP-treated tumors (Figure 1, F–H). Furthermore, treated tumors had a marked dephosphorylation of pERK and pAKT (Figure 1I). We also treated EGFR-driven TKI-sensitive LUAD immortalized cell lines HCC827 and H3255 in vitro with SMAP DT-061, a more bioavailable and potent PP2A activator (21–23). Cells were treated with DMSO control or 2.5, 5, 7.5, 10, 12.5, 15, 17.5, or 20 μM SMAP DT-061 for 48 hours. Drug treatment resulted in decreased cell viability in both cell lines, with IC$_{50}$ of 14.3 μM for HCC827 and 12.4 μM for H3255 (Supplemental Figure 2). These results indicate that PP2A activation is a viable therapeutic strategy in TKI-sensitive models of LUAD. Given the ability of these SMAPs to coordinately downregulate both AKT and MAPK signaling in culture and in vivo, we next investigated the therapeutic potential of SMAPs in TKI-resistant LUAD models, which display upregulated AKT and MAPK pathways.

PP2A activation induces apoptosis in TKI-resistant LUAD cell lines. Although initial TKI-mediated tumor regression is observed in patients with EGFR-activating mutations, resistance occurs through many mechanisms (Figure 2A), which ultimately enable the sustained activation of the MAPK and PI3K pathways. We sought to determine the effects of SMAP treatment on TKI-resistant cells and downstream signaling pathways because PP2A regulates these major downstream signaling pathways (Figure 2B). Cell viability was determined by cell counting and colony formation ability. We first treated the well-characterized TKI-resistant H1975 and H1650 human LUAD cell lines with DMSO vehicle control or 2.5, 5, 7.5, 10, 12.5, 15, 17.5,
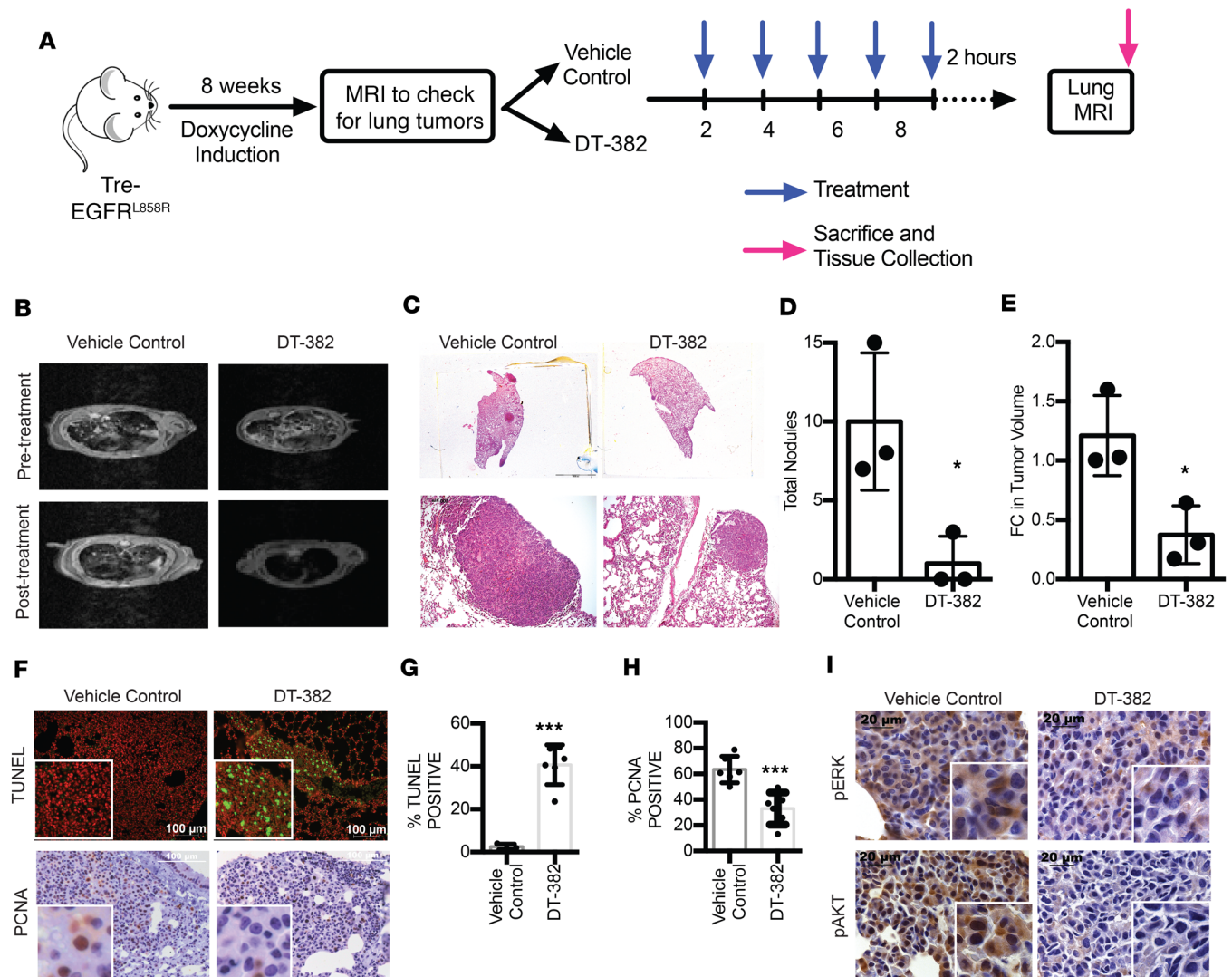
Figure 1. PP2A activation inhibits lung tumor development in an EGFR-driven TKI-sensitive non–small cell lung carcinoma transgenic model. (**A**) Expression of TRE-EGFR[L858R] was induced with doxycycline, and mice were administered either vehicle control or 100 mg/kg of SMAP every 48 hours. (**B**) Axial images obtained using MRI before and after treatment with vehicle control or SMAP. (**C**) H&E-stained sections of lung samples. (**D**) Quantification of H&E results. (**E**) Quantification of MRI results. (**F**) Immunohistochemical staining to detect apoptosis (TUNEL) and proliferation. Scale bar: 100 μm. (**G**) Quantification of TUNEL. (**H**) Quantification of PCNA. (**I**) Immunohistochemical staining of pERK and pAKT. Scale bar: 20 μm. Respective quantifications are represented as mean ± SD. *$P < 0.05$; ***$P < 0.001$.

or 20 μM SMAP DT-061 for 48 hours. Drug treatment resulted in decreased cell viability in both cell lines, with IC_{50} of 10.6 μM (Figure 2C). We then plated H1975 and H1650 at low density and treated the cells with DMSO or 2.5, 5, 7.5, or 10 μM SMAP DT-061 every 72 hours for a total of 5 treatments and stained the colonies on day 14. Treatment with SMAP DT-061 at low concentrations significantly decreased the ability of the TKI-resistant cells to form colonies (Figure 2, D–F). Treatment of cells with DMSO control or 5, 10, 20 μM SMAP DT-061 for 24 hours induced poly (ADP-ribose) polymerase (PARP) cleavage at 24 hours (Figure 2G). Because PARP cleavage is a hallmark of apoptosis, we used annexin V analysis as a second measure of programmed cell death to validate the proapoptotic effects of the small molecules. Treatment with 20 μM SMAP DT-061 for 24 hours led to a significant increase in annexin V positivity (Figure 2, H and I). The effect was neutralized by the pan-caspase inhibitor zVAD, suggesting that it is mediated by a caspase-dependent mechanism. As an additional pharmacological control, we examined the effects of DT-1310, a biologically inactive analog that lacks a N-H sulfonamide hydrogen bond donor function (Supplemental Figure 3A). Because DT-1310 is structurally similar to SMAP but is biologically inactive, treatment with DT-1310 neither induced an increase in annexin V positivity (Supplemental Figure 3B) nor inhibited
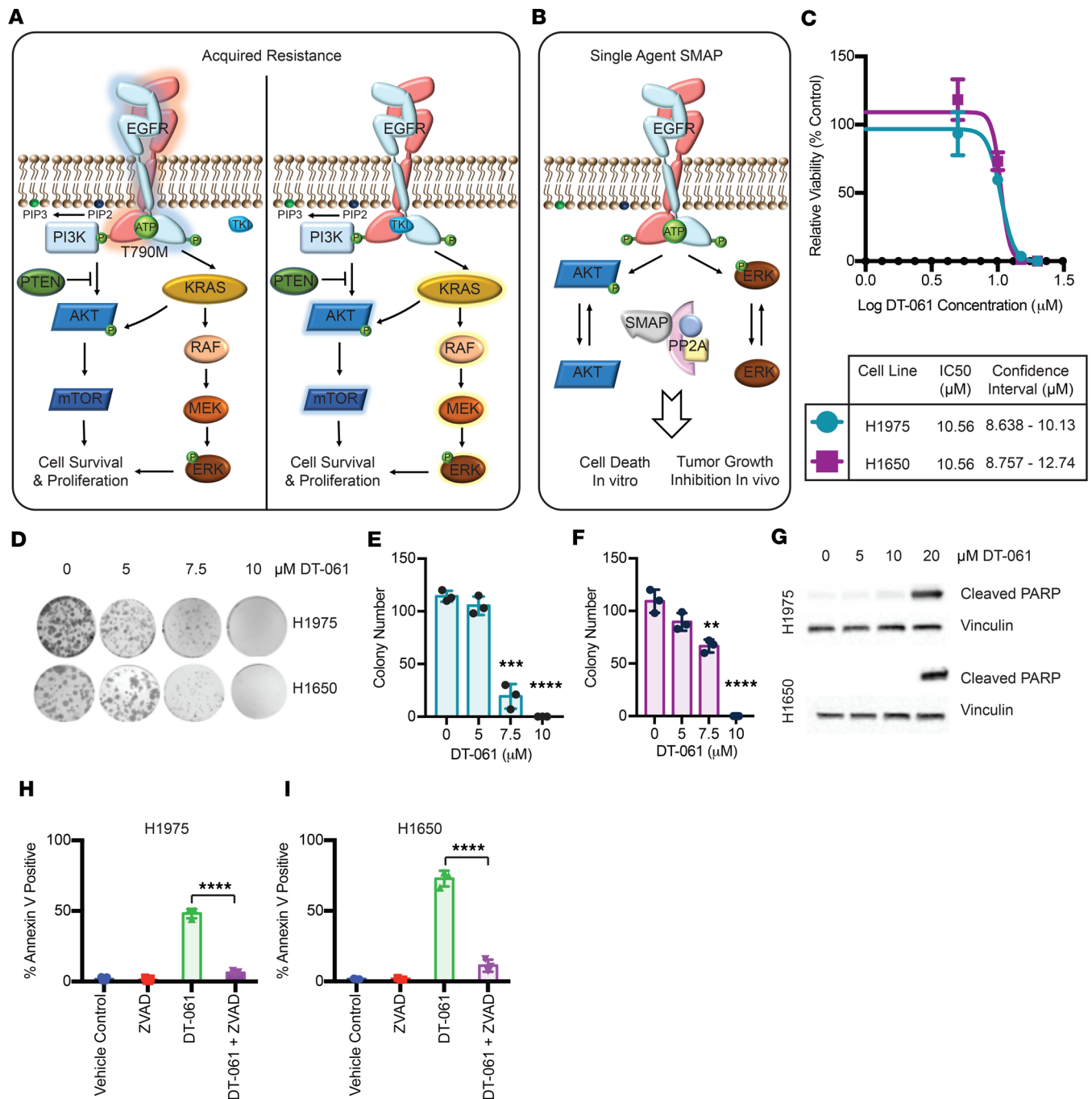
Figure 2. PP2A activation induces apoptosis in TKI-resistant LUAD cell lines. (**A**) Mechanisms of acquired resistance in LUAD. The most common mechanism of acquired resistance to TKIs is through the gatekeeper mutation T790M (tyrosine amino acid changed into a methionine at position 790), which alters the affinity of the drug to EGFR and leads to a sustained activation of both PI3K and MAPK pathways. Another common mechanism of resistance is through bypassing EGFR and sustainably activating the PI3K and MAPK pathways via modifications at the level of the downstream effectors themselves or by inactivating regulators of the pathways, such as PTEN. RAF, rapidly accelerated fibrosarcoma. (**B**) Proposed model for PP2A activation in EGFR-driven LUAD. SMAP treatment activates PP2A and leads to the downregulation of both PI3K and MAPK pathways that are commonly upregulated in TKI-resistant LUAD. (**C**) H1650 and H1975 were treated with DMSO vehicle control or increasing concentrations of SMAP DT-061 for 48 hours. Drug treatment resulted in decreased cell viability in both cell lines, with IC_{50} of 10.6 μM. (**D**) The ability of H1975 and H1650 cell lines to form colonies when treated with vehicle control or 5, 7.5, or 10 μM SMAP DT-061 every 72 hours for 14 days. (**E**) Quantification of colony formation assay for H1975. (**F**) Quantification of colony formation assay for H1650. (**G**) PARP cleavage at 24 hours in H1975 and H1650 cells treated with indicated concentrations of DT-061. Annexin positivity at 24 hours in (**H**) H1975 and (**I**) H1650 cells treated with indicated concentrations of DT-061. Three independent experiments represented as mean ± SD are shown. **$P < 0.01$; ***$P < 0.001$; ****$P < 0.0001$.

PP2A-regulated signaling pathways, such as AKT and MAPK signaling (Supplemental Figure 3C). These data further confirm the specificity of the observed effects.

PP2A reactivation overcomes TKI resistance in EGFR-driven models in vivo. The in vivo anticancer activity of SMAP was also examined in a TKI-resistant EGFR^{L858R} patient-derived xenograft (PDX) model (24). MET amplification in this TM00199 model obtained from The Jackson Laboratory is thought to confer resistance to TKI (24). Tumor fragments were surgically reimplanted in NSG female mice. Once tumor volumes reached 200 mm³, mice were randomly treated by oral gavage twice daily with vehicle control, a combination of MK2206 (6 mg/kg) and AZD6244 (24 mg/kg), or SMAP DT-061 (5 mg/kg). MK2206 and AZD6244 are kinase inhibitors that inhibit AKT and MEK, respectively. A combination of these 2 agents would lead to the inhibition of both PI3K and MAPK pathways, in comparison to the single agent SMAP that can also target both pathways simultaneously. Tumor volume was assessed 3 times weekly over 60 days. Single agent PP2A reactivation demonstrated significant, dose-dependent inhibition of disease progression in a comparable fashion to the dual AKT and MAPK pathway inhibition using the combination of kinase inhibitors (Figure 3A). SMAP DT-061 was well tolerated, had no notable toxicities, and caused no changes in body weight in the mice (Figure 3B). Mice were sacrificed 2 hours after the final treatment, and IHC detected a decrease in pERK and pAKT levels compared with vehicle control in the cancerous tissues (Figure 3C). TKI resistance was validated in this model as treatment with the TKI afatinib resulted in progressive disease (Supplemental Figure 4).

PP2A activation has an enhanced effect in combination with afatinib in an EGFR^{T790M} model. Recent reports have also shown that TKIs such as afatinib and erlotinib target the intrinsic inhibitor of PP2A, namely CIP2A (25). We decided to investigate the effect of PP2A reactivation in combination with a TKI in the context of the TKI-resistant cell lines H1975 and H1650. We first treated cells with vehicle control, 20 μM SMAP DT-061, 100 nM afatinib, 1 μM erlotinib, or a combination of SMAP DT-061 with either TKI for 24 hours. Although cells were resistant to afatinib and erlotinib, confirming their TKI-resistant status, treatment with SMAP DT-061 caused an increase in annexin V positivity compared with vehicle control (Figure 4A). Most importantly, combination of both afatinib and SMAP DT-061 had an enhanced effect on the induction of apoptosis in the H1975 harboring the T790M gatekeeper mutation (Figure 4, A and B). Thus, we decided to evaluate the effect of SMAP DT-061 and afatinib on their molecular targets and downstream effectors. Immunoblotting against EGFR, ERK, and AKT revealed an increase in dephosphorylation of AKT under afatinib and SMAP DT-061 combination treatments (Figure 4C). We also observed increased PARP cleavage with the combination of afatinib and SMAP DT-061 (Figure 4D). We sought to understand the mechanism through which pAKT is dephosphorylated to a higher extent in cells treated with the combination. Because EGFR dephosphorylation in the combination treatment was not significantly changed in comparison with either SMAP DT-061 or afatinib treatment alone, we looked at other receptors from the human EGFR family that are also targets of afatinib, and we failed to detect them using immunoblotting techniques. We examined another indirect target of afatinib, namely CIP2A. CIP2A is an endogenous inhibitor of PP2A, and its therapeutic inhibition is accompanied by a reactivation of PP2A (26). CIP2A is also the positive regulator of polo-like kinase-1 (PLK-1) (25). PLK-1 was also shown to play a role in regulating the AKT pathway (27). This mechanism is believed to explain the enhanced effect observed with the combination of the TKI and SMAP DT-061 because CIP2A was also degraded to a higher level in the combination treatment (Figure 4D). The in vivo potential of the afatinib and SMAP DT-061 combination was evaluated by administering vehicle control, SMAP DT-061 (5 mg/kg), afatinib (5 mg/kg), or a combination of both treatments (5 mg/kg each) by oral gavage in nude mice injected with H1975. Treatments were administered every 12 hours for SMAP DT-061 and every 24 hours for afatinib. Tumor volumes were measured every other day before treatment. The average tumor growth in the afatinib treatment arm was comparable to the vehicle control arm, reaching around 2,000 mm³ within 25 days. On the other hand, treatment with SMAP DT-061 significantly limited tumor growth compared with control. Finally, a combination of both small molecules had an even greater effect on tumor progression inhibition that was significantly more effective than treatment with SMAP DT-061 alone (Figure 4E). Again, the treatments were well tolerated, had no notable toxicities, and caused no changes in body weight in the mice (Figure 4F).

Our findings demonstrate that PP2A reactivation using single agent SMAP derivative is a well-tolerated and orally bioavailable therapeutic strategy that is as efficacious as a combination of kinase inhibitors in antagonizing EGFR-driven TKI-resistant LUAD models. Furthermore, treatment with SMAP can overcome resistance in those models, with an even greater effect when combined with afatinib (Figure 4G).
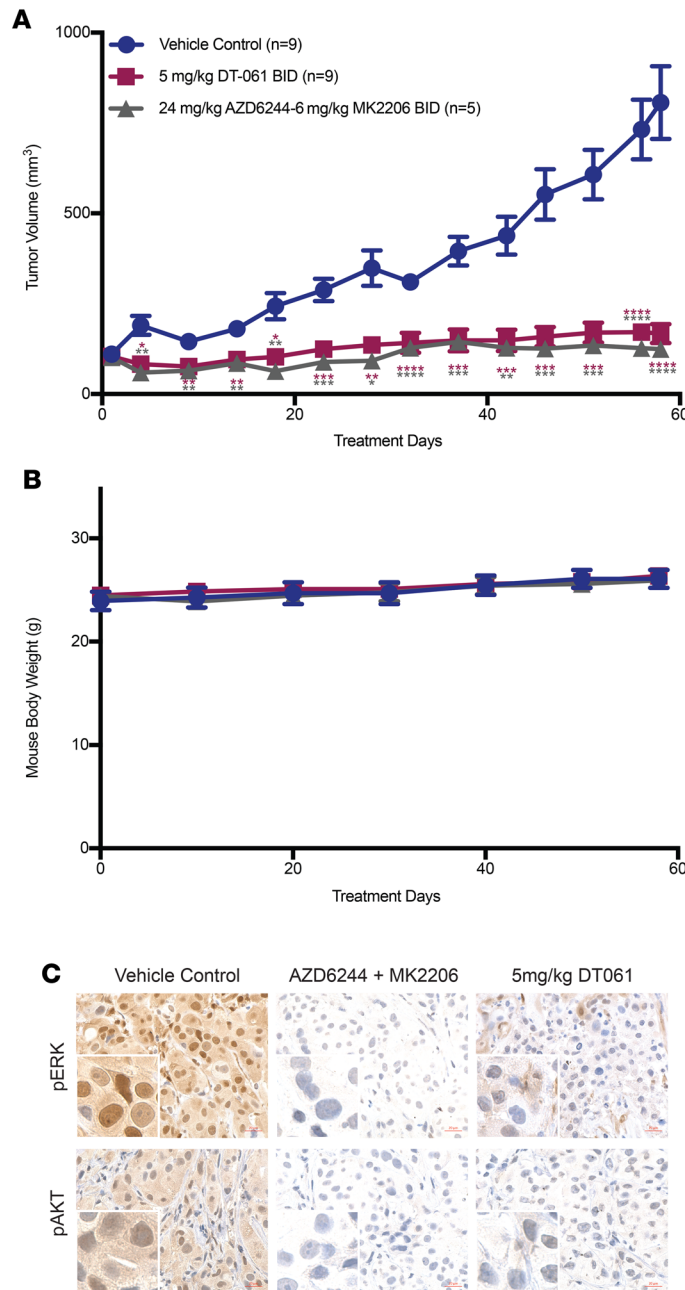
Figure 3. PP2A activation inhibits tumor growth in a TKI-resistant PDX model. (**A**) Tumor volume (mm³) in function of time in a PDX mouse model treated with vehicle control (n = 9), a combination of AZD6244 (24 mg/kg) and MK2206 (6 mg/kg) (n = 5), or SMAP2 (5 mg/kg) (n = 9). The data are represented as mean ± SEM, with *P < 0.05; **P < 0.01; ***P < 0.001; ****P < 0.0001. Gray asterisks compare the combination of AZD6244 (24 mg/kg) and MK2206 (6 mg/kg) group to the vehicle control group, while purple asterisks compare the SMAP2 (5 mg/kg) group with the vehicle control group. The P values were calculated using a 2-tailed t test. (**B**) Body weights of mice throughout the treatment. (**C**) IHC of pERK and pAKT 2 hours after the final treatment. Scale bar: 20 μm.

Discussion

These collective data support the development of PP2A activators as therapeutic agents for the treatment of TKI-resistant LUAD. Although the past decade has witnessed the development of promising targeted therapies for subsets of patients with EGFR molecular aberrations, patients develop acquired resistance to TKIs with a median time to disease progression of about a year (5, 28–31). Finding therapeutic strategies for patients who have developed resistance to first-, second-, and third-generation TKIs is an ongoing area of focus. Here, we demonstrate that PP2A activation using SMAPs is a viable strategy for both TKI-sensitive and -resistant LUAD models. Patients developing resistance to TKI exhibit various mechanisms that evade cell death. These include the amplification of either or both MAPK and PI3K pathways downstream of EGFR via mechanisms bypassing the receptor, as well as the common EGFR T790M gatekeeper mutation, which reduces the affinity of the EGFR-TKI binding (7, 8, 32, 33). The models we have used to test our hypothesis illustrate these mechanisms: (a) H1975 harbors both L858R EGFR-activating mutation as well as the gatekeeper mutation (~50% of patients); (b) H1650 possesses both activating EGFR exon 19 deletion and
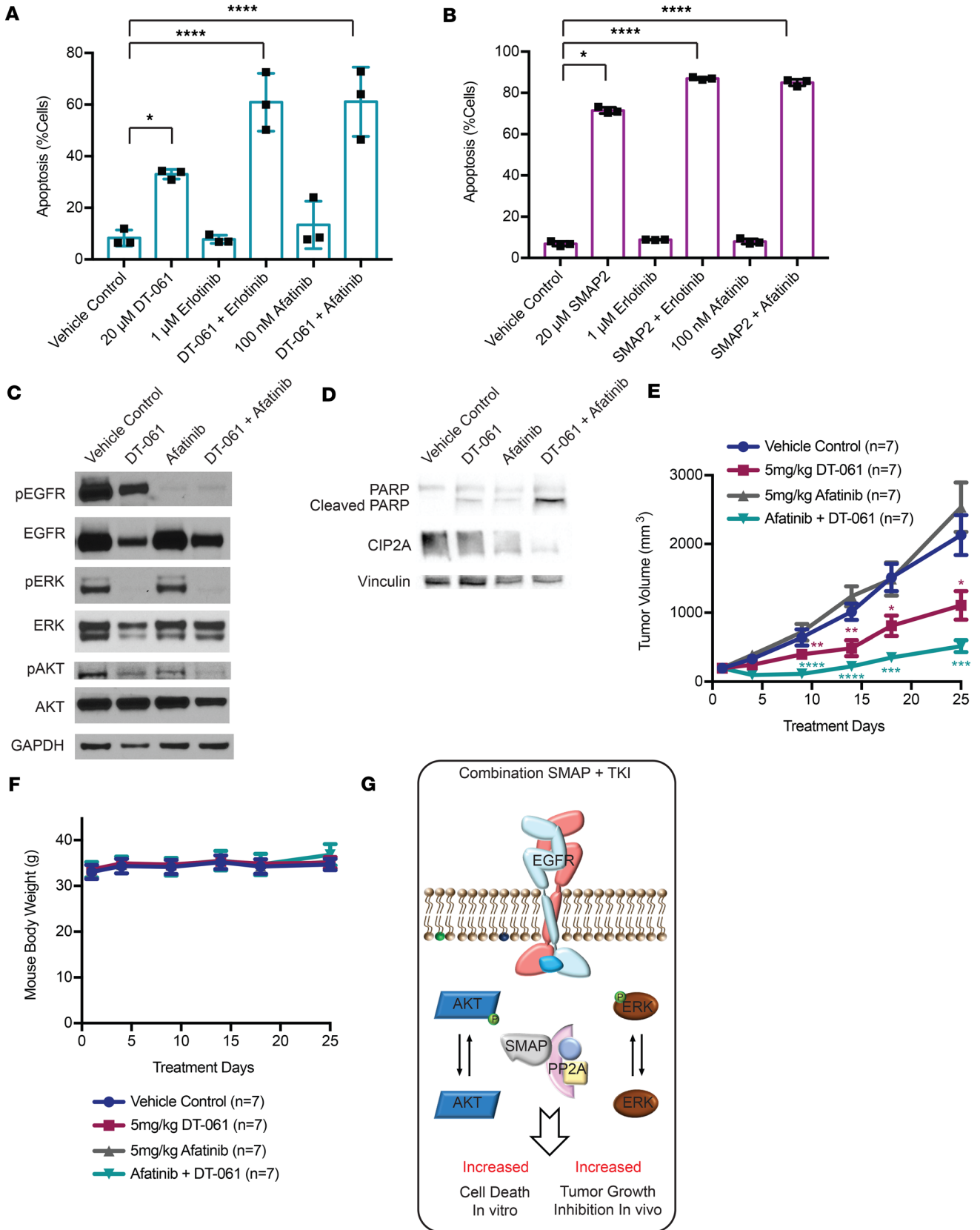
Figure 4. SMAP DT-061 in combination with TKI has an enhanced effect on apoptosis in vitro and tumor growth inhibition in vivo. (**A**) H1975 and (**B**) H1650 cell lines were treated with vehicle control, 20 μM SMAP DT-061, 1 μM erlotinib, 100 nM afatinib, a combination of SMAP DT-061 and erlotinib, or a combination of SMAP DT-061 and afatinib. Annexin positivity at 24 hours in H1975 and H1650 cells treated with indicated concentrations of DT-061. Three independent experiments are represented as mean ± SD. *$P < 0.05$; **$P < 0.01$; ***$P < 0.001$; ****$P < 0.0001$. BID: twice daily. (**C** and **D**) Western blot analysis of major PP2A and afatinib targets in H1975 treated with 20 μM SMAP DT-061, 100 nM afatinib, or a combination of SMAP DT-061 and afatinib at 24 hours. Results represent 3 independent experiments. (**E**) H1975 cells (5 million cells per injection) were subcutaneously injected in the right flank of nude mice. Once the tumor volumes reached approximately 100 mm³, mice were randomized and treated with vehicle control (n = 7), SMAP DT-061 (5 mg/kg) (n = 7) twice daily or afatinib (5 mg/kg) (n = 7) twice daily, or a combination of both SMAP DT-061 and afatinib (n = 7). The results are represented as mean ± SEM, with *$P < 0.05$; **$P < 0.01$; ***$P < 0.001$; ****$P < 0.0001$. The P values were calculated using a 2-tailed t test. (**F**) Body weights of mice throughout treatment. (**G**) Proposed model for enhanced effect of SMAP and TKI treatment of EGFR-driven LUAD. The black asterisks compare the different treatments with the vehicle control. The green asterisks compare the combination of Afatinib and DT-061 group with the vehicle control group, while the purple asterisks compare the DT-061 (5 mg/kg) group with the vehicle control group.

a PTEN deletion; and (c) the PDX model has an MET amplification, which activates downstream signals independent of EGFR (~20% of patients) (9). PTEN deletions cooccur with EGFR alterations in patients and commonly lead to the upregulation of the PI3K pathway, a mechanism of resistance observed in 5% of patients who develop acquired resistance to gefitinib or erlotinib (9). PP2A activation by SMAPs simultaneously inhibits MAPK and PI3K oncogenic signaling pathways, which are downstream targets of the phosphatase, and their dephosphorylation seems to be regulated by the cellular abundance of target proteins ERK and AKT. We have shown in our recently published work that direct therapeutic activation of a phosphatase, such as PP2A, is a potentially novel strategy that aims to concurrently target several oncogenes with a single agent (16–18). Indeed, we have found that SMAPs directly bind to and activate PP2A in KRAS-mutant LUAD, therefore inhibiting tumor growth and inducing apoptosis in mouse xenografts, PDX models, and the transgenic KRAS^{LA2} murine model (17). Furthermore, point mutations of amino acids at the putative drug-binding site completely abrogated the anticancer effect of the PP2A activator SMAP DT-061 (17). Therefore, we concluded that the observed anticancer effect is PP2A dependent. In the current study, we included a kinase inhibitor combination arm in our preclinical in vivo PDX study, and we have shown a comparable activity of SMAPs on the combination of drugs. These results underline the importance of targeting phosphatases with tumor-suppressive potential, such as PP2A. Furthermore, combination of SMAP DT-061 and afatinib had an enhanced effect on tumor growth inhibition. These findings have the potential to be extended to delaying the development of acquired resistance development by combining PP2A activator with EGFR inhibitors. To our knowledge, our SMAPs are the first generation of anticancer molecules to directly bind and activate a tumor suppressor, in this case PP2A, in the context of TKI-resistant LUAD.

Methods

Compound synthesis. SMAPs used in this study were synthesized in MO's laboratory at the Icahn School of Medicine at Mount Sinai (New York, New York, USA). SMAPs are stored at room temperature.

Cell lines and reagents. Human lung cancer cell lines were purchased from ATCC. All cells were cultured in RPMI 1640 (Thermo Fisher Scientific) supplemented with 5% FBS and 1% penicillin/streptomycin. They were maintained at less than 80% confluence and for 25 passages in incubators at 37°C with 5% CO$_2$. MK-2206 (AKT inhibitor), AZD6244 (MEK inhibitor), afatinib, and erlotinib were purchased from Selleck. These compounds were diluted in DMSO and stored at –80°C. All SMAP compounds were diluted with DMSO to a stock concentration of 80 μM and stored at room temperature. Dilutions to the treatment concentrations were made in RPMI 1640. AKT (catalog 15294) plasmid was purchased from Addgene. *Mycoplasma* testing was routinely performed using MycoAlert PLUS Mycoplasma Detection Kit (catalog LT07-710) as per manufacturer's protocol.

Antibodies. For immunoblotting, antibodies specific for pERK (catalog 9272), ERK (catalog 4695), and vinculin (catalog 4650) were obtained from Cell Signaling Technology. PARP p85 Fragment (catalog G7341) was purchased from Promega. GAPDH (catalog sc-32233) and CIP2A (catalog sc-80662) antibodies were purchased from Santa Cruz Biotechnology. For IHC, phosphorylation of ERK (Thr202/Tyr204) XP (catalog 4370) H&E, pAKT (catalog 4060), pERK (catalog 4370), and pEGFR (catalog 3777) were purchased from Cell Signaling Technology, and PCNA (catalog ab92729) was purchased from Abcam.

Western blotting. Protein was isolated from cells with RIPA Lysis and Extraction Buffer (Thermo Fisher Scientific) and from animal tissues with T-PER Tissue Protein Extraction Reagent (catalog 78510, Thermo Fisher Scientific) with cOmplete ULTRA Tablets from Roche (catalog 05892791001). Isolated protein was quantified and normalized via Bio-Rad assay (Bio-Rad). Proteins were run on 12% SDS-PAGE gels (Invitrogen, Life

Technologies) and transferred onto nitrocellulose membranes. Membranes were blocked with 5% nonfat milk (LabScientific Inc.) in Tris-buffered saline–Tween buffer. The membranes were probed with the antibodies mentioned above. Each experiment was performed in triplicate.

Cell viability and colony formation assay. For cell counting, cells were treated with the different concentrations of SMAPs for 24 hours and screened for cell viability using a Beckman Coulter cell counter. For clonogenicity (colony formation) assay, cells were plated at a low density in 6-well plates. After 24 hours, cells were treated with SMAPs every 72 hours and incubated for 14 days. Cells were then fixed and stained with 1% Crystal Violet (Sigma-Aldrich) solution. Quantification was performed through the cell counter function on ImageJ (NIH; https://imagej.nih.gov/ij/). Each experiment was plated and repeated in triplicate.

Annexin staining. Annexin V staining was performed using annexin V conjugate Alexa Fluor 488 from Invitrogen (Life Technologies) and annexin-binding buffer (catalog V13246) from Invitrogen (Life Technologies), according to the manufacturer's protocol. For cell cycle analysis, cells were stained with 7-Amino-actinomycin D (Roche) to ascertain the DNA content and determine cell cycle distribution within the cell population (34) Each experiment was performed in triplicate.

Mouse models and treatment studies. EGFR^{L858R} mice were purchased from NCI Mouse Repository. SMAP DT-382 was formulated in DMSO and delivered via intraperitoneal injection daily. For xenograft studies, H1975 (5 million cells per injection) cells were injected into the right flank of 6- to 8-week-old male BALB/c nu/nu mice (Charles River). For PDX studies, female NSG mice were purchased from The Jackson Laboratory (model TM00199). PDX tumor fragments were surgically reimplanted in the right flank of 6-week-old female NSG mice. When tumor volumes reached an average of 200 mm^3, mice were randomized to treatment groups, and tumor volume was assessed by caliper measurement every other day throughout the study. Mice were treated by gavage twice daily with vehicle control, MK2206 (6 mg/kg) and AZD6244 (24 mg/kg), or SMAP DT-061 (100 mg/kg). The reagents were formulated in a solution of N, N-dimethylacetamide/Kolliphor HS-15 (MilliporeSigma, catalog 42966-1KG)/diH$_2$O. Mice body weights were recorded weekly and percentage of mice body weights during treatment was calculated as: weight at each time point/ initial weight × 100. Animals were observed for signs of toxicity (mucous diarrhea, abdominal stiffness, and weight loss). Blood and tumor tissue was harvested 2 hours after the final dose of the treatment study. Tumors were both formalin-fixed, for IHC, and snap-frozen in liquid nitrogen, for immunoblotting.

TUNEL assay and IHC. Tissue was fixed in 10% buffered formalin phosphate (Thermo Fisher Scientific, catalog SF100-4), transferred to 70% ethanol, and blocked in paraffin. Serial tissue sections (5-μm thick) were cut from the paraffin-embedded blocks and placed on charged glass slides. Tumor sections were stained with H&E, pAKT (Cell Signaling Technology, catalog 4060), pERK (Cell Signaling Technology, catalog 4370), and PCNA (Abcam, catalog ab92729). Briefly, sections were deparaffinized with xylene and rehydrated through graded alcohol washes followed by antigen retrieval in a pressure cooker (Dako) in citrate buffer (10 μM, pH 6.0, Vector Labs). Slides were then incubated in hydrogen peroxide/methanol, followed by incubation in normal goat serum in PBS. Antibody was applied overnight at 4°C. DAB substrate was applied followed by counterstaining in hematoxylin. The ApopTag Fluorescein in Situ Apoptosis Detection Kit (Millipore) was used according to the manufacturer's protocol to perform the TUNEL assay. Before the addition of terminal deoxynucleotidyl transferase enzyme, sections were deparaffinized with xylene and rehydrated through graded alcohol washes. VECTASHIELD Mounting Medium with Propidium Iodide (Vector Labs) was used for counterstaining. Bright-field and fluorescent images were captured using an Olympus MVX10 or Zeiss Axioplan 2 IE microscope. Quantification was completed using the cell counter function of ImageJ (http://imagej.nih.gov/ij/). Imaging was performed at the Microscopy Core at the Icahn School of Medicine at Mount Sinai.

Statistics. Enhanced chemiluminescent images of immunoblots were analyzed by scanning densitometry and quantified with ImageJ (NIH) software. All values were normalized to vinculin expression and expressed as fold change relative to control. Analysis was performed using GraphPad Prism 7. Statistical significance was assumed for a 2-tailed P value of less than 0.05 using Student's t test or 2-way ANOVA with Tukey's post hoc test (presented as means; error bars indicate SD). Except where otherwise noted, box boundaries of all box-and-whisker plots represent the range of values obtained in the experiment and whiskers represent mean ± SD.

Study approval. Studies were conducted after IACUC approval (IACUC-2013-1426) at the Icahn School of Medicine at Mount Sinai and at the School of Medicine at Case Western Reserve University. Animal use and care was in strict compliance with regulatory standards and guidelines of the institutions.

Author contributions

RT designed and conducted experiments, acquired and analyzed the data, and wrote the manuscript. JS, SI, and NSD designed and conducted experiments and acquired and analyzed the data. SG, GT, SV, AT, and NV conducted experiments and acquired and analyzed the data. GN designed the research studies and interpreted the data. MO created the compounds. AM, NS, MDG, and MO provided observations and interpretations. All authors discussed the results. GN and JS provided input on the manuscript writing.

1. Siegel RL, Miller KD, Jemal A. Cancer statistics, 2017. *CA Cancer J Clin*. 2017;67(1):7–30.
2. Chen Z, Fillmore CM, Hammerman PS, Kim CF, Wong KK. Non-small-cell lung cancers: a heterogeneous set of diseases. *Nat Rev Cancer*. 2014;14(8):535–546.
3. Nakamura H, Saji H. Worldwide trend of increasing primary adenocarcinoma of the lung. *Surg Today*. 2014;44(6):1004–1012.
4. Sangodkar J, Katz S, Melville H, Narla G. Lung adenocarcinoma: lessons in translation from bench to bedside. *Mt Sinai J Med*. 2010;77(6):597–605.
5. Rosell R, et al. Screening for epidermal growth factor receptor mutations in lung cancer. *N Engl J Med*. 2009;361(10):958–967.
6. Ji H, et al. The impact of human EGFR kinase domain mutations on lung tumorigenesis and in vivo sensitivity to EGFR-targeted therapies. *Cancer Cell*. 2006;9(6):485–495.
7. Pao W, et al. Acquired resistance of lung adenocarcinomas to gefitinib or erlotinib is associated with a second mutation in the EGFR kinase domain. *PLoS Med*. 2005;2(3):e73.
8. Kobayashi S, et al. EGFR mutation and resistance of non-small-cell lung cancer to gefitinib. *N Engl J Med*. 2005;352(8):786–792.
9. Sequist LV, et al. Genotypic and histological evolution of lung cancers acquiring resistance to EGFR inhibitors. *Sci Transl Med*. 2011;3(75):75ra26.
10. Andrabi S, Gjoerup OV, Kean JA, Roberts TM, Schaffhausen B. Protein phosphatase 2A regulates life and death decisions via Akt in a context-dependent manner. *Proc Natl Acad Sci U S A*. 2007;104(48):19011–19016.
11. Silverstein AM, Barrow CA, Davis AJ, Mumby MC. Actions of PP2A on the MAP kinase pathway and apoptosis are mediated by distinct regulatory subunits. *Proc Natl Acad Sci U S A*. 2002;99(7):4221–4226.
12. Janssens V, Goris J. Protein phosphatase 2A: a highly regulated family of serine/threonine phosphatases implicated in cell growth and signalling. *Biochem J*. 2001;353(pt 3):417–439.
13. Sangodkar J, Farrington CC, McClinch K, Galsky MD, Kastrinsky DB, Narla G. All roads lead to PP2A: exploiting the therapeutic potential of this phosphatase. *FEBS J*. 2016;283(6):1004–1024.
14. O'Connor CM, Perl A, Leonard D, Sangodkar J, Narla G. Therapeutic targeting of PP2A. *Int J Biochem Cell Biol*. 2018;96:182–193.
15. Cho US, Xu W. Crystal structure of a protein phosphatase 2A heterotrimeric holoenzyme. *Nature*. 2007;445(7123):53–57.
16. Kastrinsky DB, et al. Corrigendum to "Reengineered tricyclic anti-cancer agents" [Bioorg. Med. Chem. 23 (2015) 6528-6534]. *Bioorg Med Chem*. 2015;23(23):7487.
17. Sangodkar J, et al. Activation of tumor suppressor protein PP2A inhibits KRAS-driven tumor growth. *J Clin Invest*. 2017;127(6):2081–2090.
18. Wiredja DD, et al. Phosphoproteomics profiling of nonsmall cell lung cancer cells treated with a novel phosphatase activator. *Proteomics*. 2017;17(22).
19. Kastrinsky DB, et al. Reengineered tricyclic anti-cancer agents. *Bioorg Med Chem*. 2015;23(19):6528–6534.
20. Jeong JH. Inducible mouse models for cancer drug target validation. *J Cancer Prev*. 2016;21(4):243–248.
21. van der Wekken AJ, Saber A, Hiltermann TJ, Kok K, van den Berg A, Groen HJ. Resistance mechanisms after tyrosine kinase inhibitors afatinib and crizotinib in non-small cell lung cancer, a review of the literature. *Crit Rev Oncol Hematol*. 2016;100:107–116.
22. Coco S, et al. Afatinib resistance in non-small cell lung cancer involves the PI3K/AKT and MAPK/ERK signalling pathways and epithelial-to-mesenchymal transition. *Target Oncol*. 2015;10(3):393–404.
23. Sos ML, et al. PTEN loss contributes to erlotinib resistance in EGFR-mutant lung cancer by activation of Akt and EGFR. *Cancer Res*. 2009;69(8):3256–3261.
24. Krupke DM, Begley DA, Sundberg JP, Bult CJ, Eppig JT. The mouse tumor biology database. *Nat Rev Cancer*. 2008;8(6):459–465.
25. Chao TT, et al. Afatinib induces apoptosis in NSCLC without EGFR mutation through Elk-1-mediated suppression of CIP2A. *Oncotarget*. 2015;6(4):2164–2179.

26. Kim MO, et al. Antihelminthic drug niclosamide inhibits CIP2A and reactivates tumor suppressor protein phosphatase 2A in non-small cell lung cancer cells. *Biochem Pharmacol*. 2017;144:78–89.

27. Cai XP, Chen LD, Song HB, Zhang CX, Yuan ZW, Xiang ZX. PLK1 promotes epithelial-mesenchymal transition and metastasis of gastric carcinoma cells. *Am J Transl Res*. 2016;8(10):4172–4183.

28. Lynch TJ, et al. Activating mutations in the epidermal growth factor receptor underlying responsiveness of non-small-cell lung cancer to gefitinib. *N Engl J Med*. 2004;350(21):2129–2139.

29. Paez JG, et al. EGFR mutations in lung cancer: correlation with clinical response to gefitinib therapy. *Science*. 2004;304(5676):1497–1500.

30. Pao W, et al. EGF receptor gene mutations are common in lung cancers from "never smokers" and are associated with sensitivity of tumors to gefitinib and erlotinib. *Proc Natl Acad Sci U S A*. 2004;101(36):13306–13311.

31. Mok TS, et al. Gefitinib or carboplatin-paclitaxel in pulmonary adenocarcinoma. *N Engl J Med*. 2009;361(10):947–957.

32. Engelman JA, et al. MET amplification leads to gefitinib resistance in lung cancer by activating ERBB3 signaling. *Science*. 2007;316(5827):1039–1043.

33. Bean J, et al. MET amplification occurs with or without T790M mutations in EGFR mutant lung tumors with acquired resistance to gefitinib or erlotinib. *Proc Natl Acad Sci U S A*. 2007;104(52):20932–20937.

34. Sangodkar J, et al. Targeting the FOXO1/KLF6 axis regulates EGFR signaling and treatment response. *J Clin Invest*. 2012;122(7):2637–2651.